J Mater Sci (2006) 41:6813–6821
DOI 10.1007/s10853-006-0211-8

Analysis of interfacial micromechanics of model composites using synchrotron microfocus X-ray diffraction

Y. T. Shyng · J. A. Bennett · R. J. Young · R. J. Davies · S. J. Eichhorn

Published online: 12 August 2006

Abstract The deformation micromechanics of single-fibre embedded model composites of poly(*p*-phenylene benzobisoxazole) (PBO) and poly(*p*-phenylene terephthalamide) (PPTA) fibres, embedded in an epoxy resin have been examined using synchrotron microfocus X-ray diffraction. Single fibres (in air) were deformed and the *c*-spacing monitored to establish a calibration of crystal strain against applied stress. Subsequently, the variation in crystal strain along fibres, embedded in the resin matrix was mapped using synchrotron microfocus X-ray diffraction. Raman spectroscopy was then used to map molecular deformation on the same samples (recorded as shifts in the Raman band wavenumber) in order to provide a complementary stress data. A shear-lag analysis was conducted on the axial fibre stress data in order to calculate interfacial shear stress and identify different stress-transfer modes at fibre/resin interfaces. The results establish that the axial fibre stress distributions measured by synchrotron microfocus X-ray diffraction correlate well with those obtained using Raman spectroscopy. The interfacial shear stress data derived from the stress-transfer profiles also show a good degree of correlation.

Y. T. Shyng · J. A. Bennett · R. J. Young (✉) · S. J. Eichhorn
Materials Science Centre, School of Materials,
University of Manchester, Grosvenor St.,
Manchester M1 7HS, UK
e-mail: Robert.young@Manchester.ac.uk

R. J. Davies
European Synchrotron Radiation Facility, B.P. 220, F-38043
Grenoble, Cedex, France

Introduction

An engineering composite material may be considered as two or more physically distinct materials, combined with the purpose of achieving properties, which are unique and/or superior to those of the component materials. The design and production of high-performance fibre reinforced polymers, one of the main categories of composite materials, is based upon this ideal. The properties of these composite materials are dependent upon the properties of the individual components and those of the key fibre/matrix interface region. In particular, the properties of the interface may be varied to control the fracture toughness, fatigue resistance, stiffness and strength of the composite.

Of the various methods, which have been established to determine the properties of the fibre/matrix interface, one of the most commonly used is the single-fibre fragmentation test [1]. This test relies on the properties of the fibre, matrix and the interface being balanced in such a way as to permit fragmentation of a long continuous fibre into critical lengths [1]. It is simple to perform in the classical set-up, requiring only an estimate of the average fibre fragment length, number of fragments and a measurement of peak load. The end result is a single interfacial shear strength (τ_i) value, making comparison between different matrix/fibre systems easy. However, our previous studies have shown that the assumed form of the interfacial shear stress distribution is too simple for many composite systems and can lead to a gross miscalculation [2, 3].

Raman spectroscopy has been used extensively to evaluate the micromechanical interfacial properties of fibre reinforced composite materials [1]. This approach makes it possible to measure the point-to-point variation in axial stress along a fibre embedded in a resin matrix. In this kind of study, a model composite is loaded in stages and the

axial stress is measured at discrete points along the fibre, by monitoring changes in stress sensitive Raman band positions, at each stage of the process. The interfacial shear stress can then be calculated by using a balance of forces argument [4], thus allowing progressive interfacial failure processes to be accurately monitored. Recently [5] a synchrotron X-ray based strain scanning technique has been specifically developed to monitor the stress/strain distributions within two-phase systems of oriented and non-oriented polymeric materials. The results of this work show that this technique is particularly useful for interfacial characterisation of fibre reinforced polymer composites.

In this study, single-fibre model composites were examined by both synchrotron radiation and Raman spectroscopy. In each case the variation of axial fibre stress was mapped along a fibre embedded in a polymeric matrix. Subsequently, the corresponding interfacial shear stress values were calculated from the measured axial fibre stress distributions.

Interfacial analyses theories

Stress transfer—elastic model

The shear-lag model originally proposed by Cox [4] can be used to model the distribution of fibre strain in a single-fibre model composite, where the fibre is short or discontinuous (e.g. in a fragmentation test [1]). The model assumes that the fibre and matrix are in an elastic state and that there is perfect adhesion along the interface. The variation in axial fibre stress (σ_f), with position (x) along an embedded fibre is given as follows [6]

$$\sigma_f = e_m E_f \left[1 - \frac{\cosh(n x / r_f)}{\cosh(ns)}\right] \quad (1)$$

where e_m is the matrix strain, E_f is the fibre modulus and r_f is the fibre radius. The parameter s is the fibre aspect ratio $l/2r_f$, where l is the fibre length. The parameter n is dimensionless and can be expressed as follows

$$n^2 = \frac{E_m}{E_f} \frac{1}{\ln(R/r_f)} \frac{1}{(1+\upsilon_m)} \quad (2)$$

where E_m is matrix modulus, v_m is the matrix Poisson's ratio and R is the radius of a solid cylinder of matrix around the fibre that is influenced by the applied stress. Using a force balance approach [7] enables the rate of change of fibre stress with respect to the position along an embedded fibre to be calculated using the expression

$$\frac{d\sigma_f}{dx} = -\frac{2\tau}{r_f} \quad (3)$$

where τ is the interfacial shear stress.

Hence, an expression for the variation of interfacial shear stress along the fibre can be derived such that

$$\tau = \frac{n\, e_m\, E_f}{2} \frac{\sinh(n x / r_f)}{\cosh(ns)} \quad (4)$$

Stress transfer—debonded model

Kelly and Tyson [8] proposed a model that can be used to describe the distribution of stress along a fibre, which has debonded from the matrix. In this case, the interface is assumed to be the debonded along the whole fibre length and the stress induced by applied deformation is transferred from the matrix to the fibre as a frictional sliding stress (τ_f). Kelly et al. assumed that τ_f is constant and thus the stress distribution along the embedded fibre in the debonded region can be expressed as follows

$$\sigma_f = \frac{2\,\tau_f}{r_f}\left(\frac{1}{2} - x\right) \quad (5)$$

As the value of τ_f has to be a constant, the axial fibre stress distribution is linear instead of the curved profile found in the elastic region. This theory has been verified experimentally for a number of polymeric fibre/matrix systems using Raman spectroscopy [6].

Partial debonding

The partial-debonding model was proposed by Piggott [9], for the case when the shear stress at a discontinuity such as the fibre end, rises to such a high value that interfacial failure occurs along part of the fibre. The partial-debonding model combines the theories of Cox [4] and Kelly and Tyson [8], using Eqs. 1 and 5 to calculate profiles in the bonded and debonded regions, respectively.

Experimental

Materials

Fibres

Two high performance fibres were chosen for this study, namely poly(*p*-phenylene terephthalamide) (PPTA) and

poly(*p*-phenylene benzobisoxazole) (PBO). The molecular structures of both fibres are shown in Fig. 1. The PPTA fibres, which have a Youngs modulus, E_f, of 105 GPa, were supplied by Teijin Co Ltd. under the tradename Twaron. The PBO fibres, which have a Youngs modulus, E_f, of 260 GPa, were supplied by Toyobo Co. Ltd under the name Zylon.

Matrix

A cold-curing two-part epoxy resin was chosen for the matrix material. The epoxy resin, supplied by Ciba Geigy, UK, consisted of 100 parts by weight of butane-1,4-diol diglycidyl ether resin (LY5052) and 38 parts by weight of isophorone diamine hardener (HY5052). The resin was cured at room temperature for 7 days.

Fibre diameter determination

A Philips 525 M scanning electron microscope (SEM) was used to determine fibre diameters. At least 20 fibres of each type were selected at random and examined at three different magnification levels. Diameters were estimated for each fibre by comparing with a standard SEM graticule. The fibre diameters were found to be 12.1 ± 0.5 μm and 11.2 ± 0.7 μm for the PPTA and PBO fibres, respectively.

Single-fibre embedded model composite preparation

A square 'picture-frame' mould was used to prepare an epoxy resin plate with isolated, embedded single-fibres. PPTA and PBO single fibres were carefully cut into a number of ~10 mm lengths. The square 'picture frame' mould was half filled with resin and allowed to cure partially before the individual 10 mm fibre lengths, were placed on the surface of the resin. The fibres were encapsulated by adding more resin to the mould. The mould was then kept at room temperature for seven days in order to allow complete curing of the epoxy resin. Individual samples were machined from the square epoxy resin plate, into dumb-bell test specimens, with the fibre axis lying parallel to the tensile axis of the specimen, as shown in Fig. 2. The gauge length and the thickness of the specimens were 50 and 2 mm, respectively.

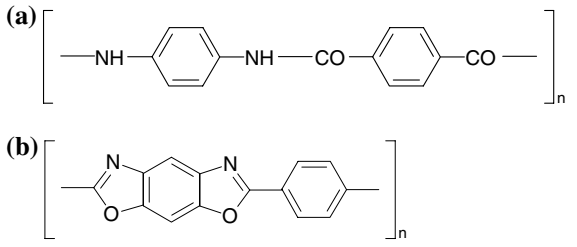

Fig. 1 Polymeric structures of (**a**) PPTA and (**b**) PBO fibres

Synchrotron radiation diffraction methods

General background

Synchrotron radiation which is well known for its high brilliance, deep penetration and microfocus capability, has been widely used in different fields. An earlier study on determining the crystal modulus of PBO fibres [10] demonstrated the usefulness of synchrotron radiation and confirmed the potential of microfocus X-ray diffraction (XRD) as a tool for monitoring deformation in oriented polymer systems. The present study utilised a synchrotron XRD set-up, on beamline ID13, at the European Synchrotron Radiation Facility (ESRF). This beamline is configured with a Kirkpatrick-Baez (KB) type mirror, and is collimated using a piezo-based block system. This provides an on-sample beam spot-size of approximately 5 μm, with a radiation wavelength of 0.095 nm. A CCD detector with an average pixel size of 257.79 μm^2 was used to capture diffraction patterns.

Experimental configuration—model composites

A miniature materials tensile testing rig was used for sample deformation. The samples were fixed to the rig using a grip mechanism with pins inserted through the holes at either end of the dumbbell sample (shown in Fig. 2) to limit slippage. Initially a small load was applied to each sample to ensure it was mounted securely within the grips, thus ensuring the position of the sample did not change significantly during subsequent loading steps. Deformation was applied to the samples in steps using a manually controlled gearbox. The stress applied to the sample, σ_{app}, was estimated from measurements of local fibre stress, σ_f, near the middle of the fibre. By calculating the fibre strain, e_f, and assuming this to be equal to the strain in the matrix [7],

$$\sigma_{app} = \sigma_m = \frac{E_m}{e_m} \tag{7}$$

where E_m is the matrix modulus and σ_m is the matrix stress.. The deformation at each step is subsequently referred to in terms of a nominal applied load σ_{app}.

Diffraction patterns were generated along the embedded fibre length at various levels of applied stress, and at 25 and 20 μm intervals along fibres embedded in PPTA and PBO composite samples, respectively. The diffraction patterns retrieved for the model composite were a combination of

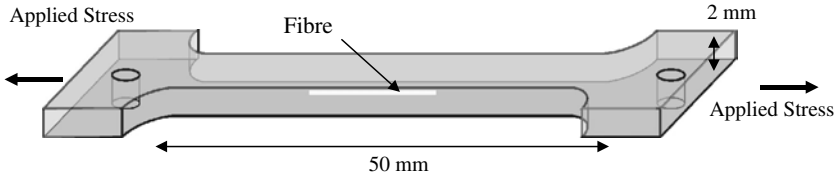

Fig. 2 Schematic of a single-fibre model composite

epoxy and fibre patterns. It has been shown elsewhere how the resin diffraction patterns for epoxy can be subtracted from bulk patterns, leaving only the fibre layer lines, which can be used for *c*-spacing determinations [5]. The same method was employed in the present study. All diffraction patterns were taken using an exposure time of 10 s. The sample-to-film distance was calculated from the diffraction pattern of an Al_2O_3 calibration sample.

Determination of crystal strain

Analysis of the diffraction data was performed using the FIT2D software application [10]. Radial profiles of intensity as a function of distance, h, from the beam centre were first generated along the meridional axis thus allowing the positions of the fibre crystallographic reflections to be determined. This enables the subsequent calculation of lattice spacings in the fibre axis direction (commonly referred to as *c*-spacings). These were calculated using one-dimensional diffraction grating theory according to [11].

$$c = \frac{n_l \lambda}{\sin\left[\tan^{-1}\left(\frac{h}{r}\right)\right]} \tag{8}$$

where n_l is the order of diffraction, λ is the X-ray wavelength, r is the sample-to-detector distance, and h is the reflection distance from the beam centre. A more detailed description of a similar analysis procedure has previously been reported elsewhere [12]. Crystal strain may then be calculated as the change in lattice spacing during sample deformation [13]. Calibration curves were obtained, from single-fibre samples deformed on a custom built stress rig, by recording diffraction patterns at incrementally increasing levels of fibre stress.

Raman spectroscopy methods

General background

The samples used for the synchrotron experiment were retrieved and the axial fibre stresses were mapped in a similar fashion using Raman spectroscopy, which can be used to measure stress variations along single fibres, such as PPTA or PBO, embedded inside transparent epoxy resins [14]. Both PPTA and PBO fibres possess strongly deformation sensitive Raman bands located at 1610 and 1618 cm^{-1}, respectively [15]. This reflects the fact that in such materials macroscopic deformation of the fibres is translated directly into the stretching of the covalent bonds of the highly aligned molecules. Both peaks shift towards a lower wavenumber when the fibre is experiencing tensile stress, hence a Raman band shift rate can be obtained and used as a calibration of deformation. The fibre stress, σ_f, at a discrete point along a fibre embedded in a composite can then be estimated by analysing a Raman spectrum taken from that point and using the calibration to calculate the appropriate value.

Experimental configuration—model composites

A Renishaw Raman spectroscopy system was employed in this experiment. Raman spectra of single-fibres embedded in model composites were taken using a 25 mW He–Ne (632.8 nm) laser. A modified Olympus optical microscope with a 50× objective lens was used, and the laser power measured at the surface of the material was about 1.3 mW. Each spectrum was obtained with a 2 s exposure time using a highly sensitive Charge Couple Device (CCD) camera.

The single-fibre embedded model composites were deformed using the same testing rig used in the synchrotron experiments. As in the synchrotron XRD experiments, the level of applied tensile deformation was observed by monitoring the stress in the middle of the fibre, assuming that the strain in the fibre is equivalent to the strain in the matrix. Tensile deformation was carefully applied to the sample in several steps. Raman spectra were recorded along the embedded fibre length at various levels of applied stress, and at 20 and 25 μm intervals along fibres embedded in PPTA and PBO composite samples, respectively.

Deformation experiments

Synchrotron radiation

Stress calibration

Figure 3 shows typical diffraction patterns obtained for the PPTA and PBO fibres in air, as used in this study. The strong equatorial reflections and multiple meridional reflections indicate a high degree of crystallite orientation along the fibre axis and suggest good lateral packing of the stiff-molecules within the fibre. The (002) and (004) layer

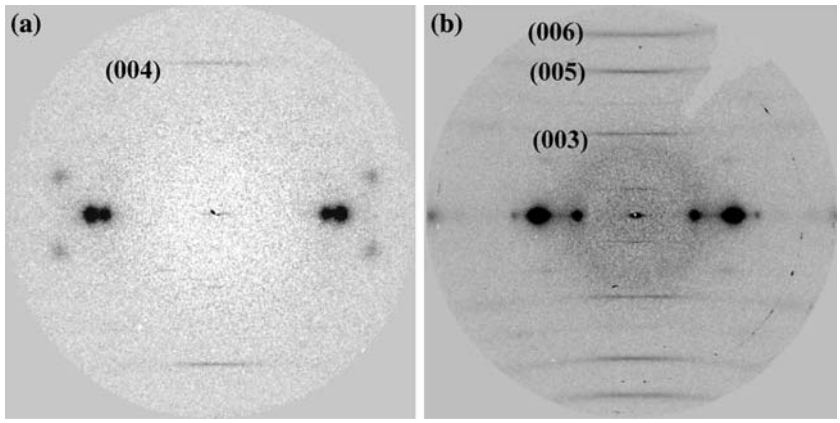

Fig. 3 Synchrotron diffraction patterns for (**a**) a PPTA and (**b**) a PBO fibre

lines are visible in the PPTA diffraction pattern whereas the PBO diffraction pattern exhibits well-defined (003), (005) and (006) layer lines. It is these meridional reflections which are used to determine the axial crystal strain. For PPTA only the well defined (004) reflection was used to calculate *c*-spacing. However, for PBO it was possible to improve the accuracy of the result by using both (005) and (006) reflections. Due to constant corrections that were required in order to maintain the beam alignment, small changes in the beam centre position could occur. To overcome this, reflections both above and below the beam centre were used to extract peak position, and then an average was taken. In this way, any small vertical changes in beam position would be cancelled out. The results of the axial fibre stress calibration and crystal modulus determination for PPTA and PBO fibres are shown in Fig. 4. The PPTA crystal modulus, $E_{\mathrm{fc,}}$ is reported to be approximately 220–290 GPa [16], which is consistent with the 224 ± 3 GPa result obtained in this study. As can be seen, the PBO fibre has a crystal modulus of 469 ± 7 GPa, which is in good agreement with earlier estimates, which report the value to be 430–460 GPa [11, 17]. The stress calibrations obtained here are used to relate the crystal strain to the stress in the fibre within the model composite. The crystal modulus of both fibre types was found to be significantly greater than typical Young's modulus values, $E_{\mathrm{f}} = 105$ and 260 GPa, for PPTA and PBO, respectively. This gives an indication of the influence of factors which can cause a reduction in the measured tensile modulus of the fibres, such as flaws, voids, impurities and poor crystallite orientation.

PPTA–epoxy composite micromechanics

The axial fibre stress distributions for the PPTA single-fibre embedded model composite, measured by synchrotron XRD, are shown in Fig. 5. Measurements were made at four different loading levels, each identified by an applied stress, σ_{app}. Each point represents the stress derived from an individual diffraction pattern, taken at a discrete point along the fibre, some distance x from the fibre end.

The data shown in Fig. 5 demonstrate how the stress distribution along the fibre changes when deformation is applied to the sample. At $\sigma_{\mathrm{app}} = 3$ MPa the stress distribution is approximately flat and close to zero. As the σ_{app} is increased through 17, 25 and 34 MPa, it can be seen that the stress along the fibre also increases, rising sharply from the fibre end before levelling off to a plateau value at some distance x along the fibre. The plateau stress values of the PPTA model composite at the initial loading levels are 0.1, 0.6, 0.9 and 1.2 GPa, respectively. These stress distributions, which are qualitatively similar to the shear-lag distributions described in section Stress transfer—elastic model, indicate that the fibre/matrix interface is deforming elastically and hence remains fully bonded. This correlation is confirmed by the theoretical curves, calculated from Eq. 1, fitted to the data in Fig. 5. The curves were adjusted to give the best fit to the experimental data by varying the shear-lag fitting parameter, n, which is listed within the inset box, along with relevant material properties.

The corresponding interfacial shear stress distributions derived using Eq. 3 are shown in Fig. 6. It can be seen that in each case the interfacial shear stress is highest at the fibre end, progressively tending to zero with distance x along the fibre. Maximum τ_{i} values at $\sigma_{\mathrm{app}} = 3$, 17, 25 and 34 MPa in the PPTA model composite, were found to be 5, 18, 22 and finally 28 MPa, respectively.

PBO–epoxy composite micromechanics

The experimental data showing the variation in axial fibre stress along a PBO single-fibre embedded in an epoxy resin matrix, measured by synchrotron XRD, are presented in Fig. 7. Deformation was applied in four steps and synchrotron diffraction patterns were recorded as described in section Experimental configuration—model composites. A small amount of stress, 0.15 GPa, is induced in the fibre by the residual deformation, $\sigma_{\mathrm{app}} = 2$ MPa. However, the

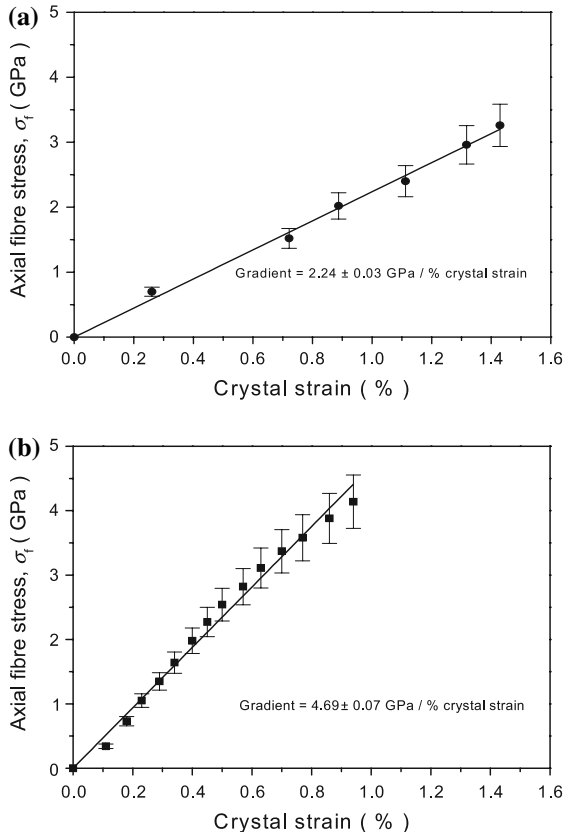

Fig. 4 Fibre stress calibrations of (**a**) PPTA and (**b**) PBO fibres

profile remains approximately flat. As σ_{app} is increased through 12, 16 and 24 MPa, the stress along the fibre can be seen to rise sharply from the fibre end before levelling off to a plateau value at some distance x along the fibre. The plateau stress values of the PBO model composite for each successive increase in σ_{app} are 0.15, 1, 1.4 and 2.1 GPa, respectively. The theoretical curves, calculated from Eq. 1, also shown in Fig. 7, confirm that the stress

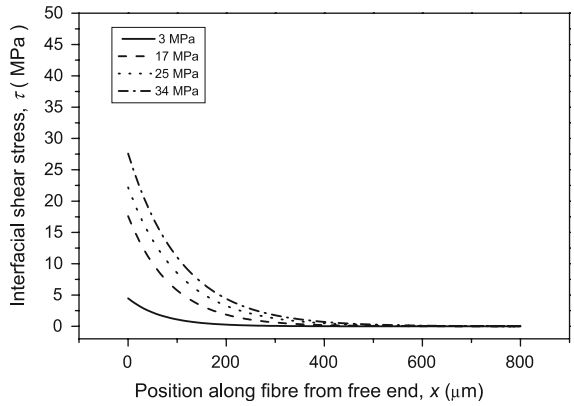

Fig. 6 Interfacial shear stress distributions along a PPTA fibre embedded in an epoxy resin matrix subjected to increasing levels of loading (derived from theoretical shear-lag model in Fig. 5 using Eq. 3)

distributions correlate well with the elastic shear-lag analysis described in section Stress transfer—elastic model, thus indicating that the fibre/matrix interface remains fully bonded. As before the curves were adjusted to give the best fit to the experimental data by varying the shear-lag fitting parameter, n, which is listed within the inset box, along with relevant material properties.

Figure 8 shows the interfacial shear stress distributions corresponding to the results in Fig. 7. The values of τ_i for σ_{app} = 2, 12, 16 and 24 MPa loading levels are 7, 31, 41 and finally 46 ± 5 MPa, respectively. The maximum value of the shear stress (46.0 MPa) slightly exceeds the shear yield stress of the resin [18], and corresponds to values reported elsewhere for PBO/epoxy [19] systems. Since there is no evidence of interfacial failure it can be assumed there is a good interfacial bond between fibre and matrix, however elastic stress transfer behaviour must be limited by the onset of matrix plasticity and hence it is possible that some limited matrix yielding has taken place very

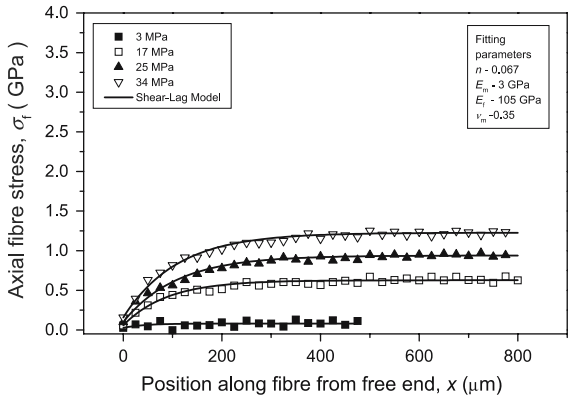

Fig. 5 Stress distributions along a PPTA fibre embedded in an epoxy resin matrix subjected to increasing levels of loading measured by synchrotron radiation (fitting parameters for theoretical shear-lag curves shown in box)

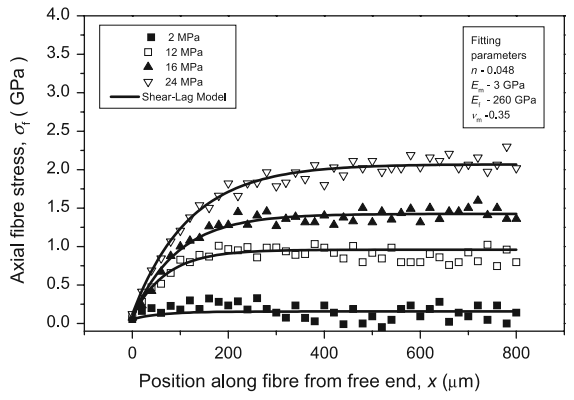

Fig. 7 Stress distributions along a PBO fibre embedded in an epoxy resin matrix subjected to increasing levels of loading measured by synchrotron radiation (fitting parameters for theoretical shear-lag curves shown in box)

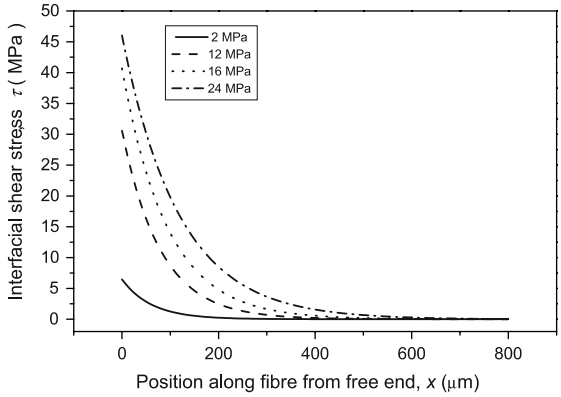

Fig. 8 Interfacial shear stress distributions along a PBO fibre embedded in an epoxy resin matrix subjected to increasing levels of loading (derived from theoretical shear-lag model in Fig. 7 using Eq. 3)

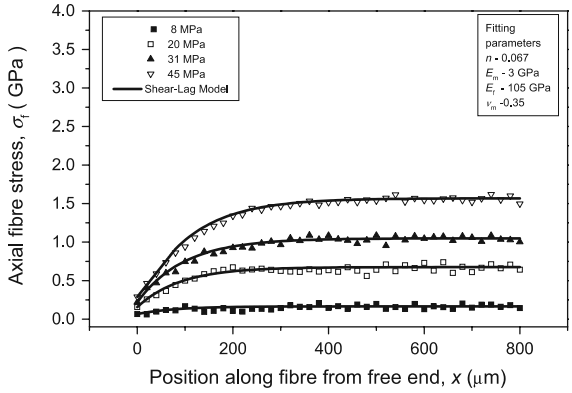

Fig. 9 Stress distributions along a PPTA fibre embedded in an epoxy resin matrix subjected to increasing levels of loading measured by Raman spectroscopy (fitting parameters for theoretical shear-lag curves shown in box)

close to the fibre end, which is beyond the resolution of the present technique.

Raman spectroscopy

Single-fibre stress calibration

The measured stress induced band shift rates for the 1610 and 1618 cm^{-1} Raman peaks, from PPTA and PBO fibres, respectively, are presented in Table 1. These values were used as a calibration of local deformation in the fibre encapsulated within the epoxy resin matrix.

PPTA–epoxy composite micromechanics

The experimental data representing the variation in axial fibre stress, measured by Raman spectroscopy, along the fibre, in the same PPTA/epoxy single-fibre model composite used for the synchrotron study (reported in section PPTA–epoxy composite micromechanics), are presented in Fig. 9. The measured length along the fibre was 800 μm, with intervals of 20 μm between measurements. As with the synchrotron experiment, deformation was applied in four steps, σ_{app} = 8, 20, 31 and 45 MPa. The use of Raman spectroscopy to monitor the micromechanics gives similar stress distributions to those obtained using the synchrotron diffraction approach, with stress building up from the fibre end before levelling off to a plateau value. In this case the plateau values for each of the applied stress levels are 0.3, 0.7, 1.1 and 1.6 MPa, respectively. It was possible to fit the experimental data, using typical fitting parameters, with the theoretical shear-lag model up to σ_{app} = 31 MPa, thus indicating the stress transfer is taking place elastically. Thereafter, a short linear region in the stress distribution, extending from the fibre end over a distance of about 80 μm, can be seen to develop, when σ_{app} is increased to 45 MPa. The linear region indicates the onset of inelastic behaviour such as matrix yielding or fibre/matrix debonding. Equations 5 and 6 have been used to generate and fit the experimental data with the theoretical partial-debonding model, first described by Piggott [9]. It should be noted that the level of applied deformation is higher than that applied during the synchrotron experiment.

Detailed interfacial shear stress distributions for each level of applied deformation are shown in Fig. 10. The maximum interfacial shear stresses for each deformation step are 3.9, 18, 29 and 27 ± 3 MPa, respectively, and are good in agreement with the synchrotron data. In the inelastic region, indicated in Fig. 10, it can be seen that the interfacial shear stress is estimated to be 24 MPa. The small drop in τ (at σ_{app} = 45 MPa) from the maximum value of 27–24 MPa in the inelastic region seems to indicate that a yielding process has been initiated.

Table 1 Stress and strain induced Raman band shift rates for PBO and PPTA fibres

Fibre type	Stress-induced shift rate (cm^{-1}/GPa)	Strain-induced shift rate (cm^{-1}/%)
PPTA	–3.9 ± 0.3	–3.6 ± 0.3
PBO	–3.1 ± 0.2	–7.5 ± 0.4

PBO–epoxy composite micromechanics

The experimental data representing the variation in axial fibre stress, measured by Raman spectroscopy, along the fibre in the same PBO/epoxy single-fibre model composite used for the synchrotron study (reported in section PBO–epoxy composite micromechanics), are presented in Fig. 11. Four different levels of applied matrix stress, σ_{app} = 3, 16, 22 and 33 MPa, were used in order to compare with the synchrotron diffraction results. The overall

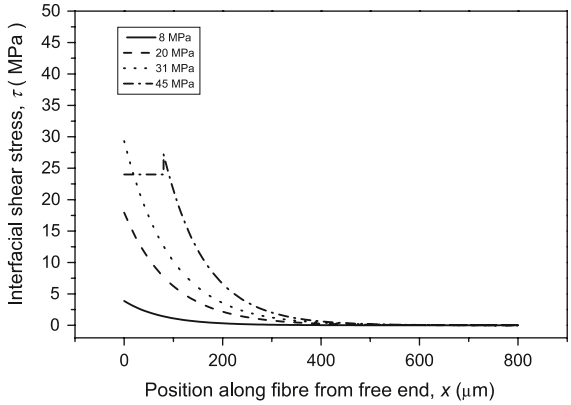

Fig. 10 Interfacial shear stress distributions along a PPTA fibre embedded in an epoxy resin matrix subjected to increasing levels of loading (derived from theoretical shear-lag model in Fig. 9 using Eq. 3)

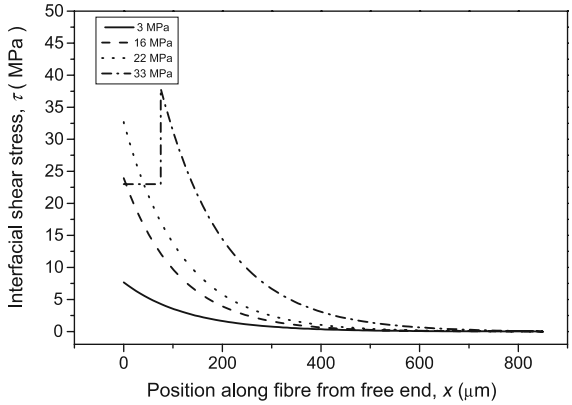

Fig. 12 Interfacial shear stress distributions along a PBO fibre embedded in an epoxy resin matrix subjected to increasing levels of loading (derived from theoretical shear-lag curves in Fig. 11 using Eq. 3)

length of fibre mapped was 850 μm at intervals of 25 μm. As with the PPTA samples, the measured data representing variation of axial fibre stress, obtained using Raman spectroscopy are consistent with those measured by synchrotron diffraction. Axial fibre stress distributions for each successive deformation level reach plateau values of 0.3, 1.4, 1.9 and 2.9 GPa. In this case it was possible to use the theoretical elastic stress transfer curves to fit the experimental data, using typical fitting parameters, up to σ_{app} = 22 MPa. During the final deformation step, σ_{app} = 33 MPa, there is clear evidence of a significant region of interfacial failure, characterised by a linear inelastic region in the stress distribution, which can be clearly identified. The length of the inelastic region is approximately 75 μm. It can be seen that the theoretical partial-debonding curve [9] fits the data well. The applied stress at which the inelastic behaviour occurs, σ_{app} = 33 MPa, is higher than the maximum applied during the synchrotron experiments.

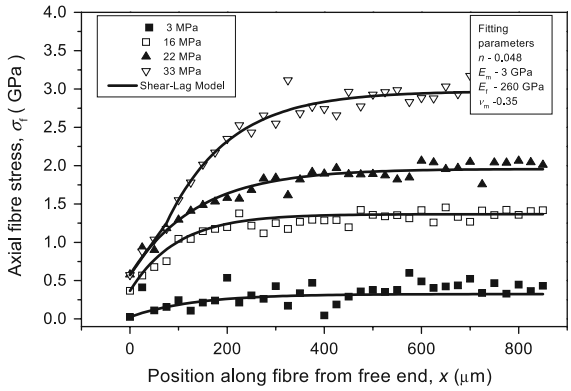

Fig. 11 Stress distributions along a PBO fibre embedded in an epoxy resin matrix subjected to increasing levels of loading measured by Raman spectroscopy (fitting parameters for theoretical shear-lag curves shown in box)

The corresponding interfacial shear stress distributions are shown in Fig. 12. The maximum interfacial shear stresses obtained using this method were 8, 24, 33 and 38 ± 4 MPa. These results are in line with previous experiments on PBO/epoxy systems [19]. By contrast to the PPTA/epoxy system, there is a larger drop in interfacial shear stress (at σ_{app} = 33 MPa) from a maximum value of 43–23 MPa. In this case, the size of the drop appears to indicate that interfacial failure is due to fibre/matrix debonding.

Conclusions

High quality synchrotron diffraction patterns acquired using the XRD set-up have been obtained for single high performance polymeric fibres. By correlating crystal strain data derived from these patterns with the applied fibre stress is has been possible to construct calibration curves, for use in evaluating the stress distributions along fibres, within model composites. The crystal moduli estimated from the calibration curves were 224 and 469 GPa for the PPTA and PBO fibres, respectively. Axial fibre stress distributions were successfully obtained by synchrotron XRD. The data obtained show the micromechanical behaviour of the fibre/matrix interface, which is typical of elastic stress transfer for PPTA and PBO fibre model composites. This observation was further substantiated, by a good correlation between the experimental data and theoretical curves representing classical shear-lag analyses.

Both the PPTA and PBO single-fibre embedded model composites were retained and subsequently re-examined using a Raman spectroscopy approach to stress mapping. By determining the Raman band shift rate, the axial fibre stress distribution along the fibres was obtained. At similar levels of applied deformation good agreement was found between the Raman and synchrotron XRD data.

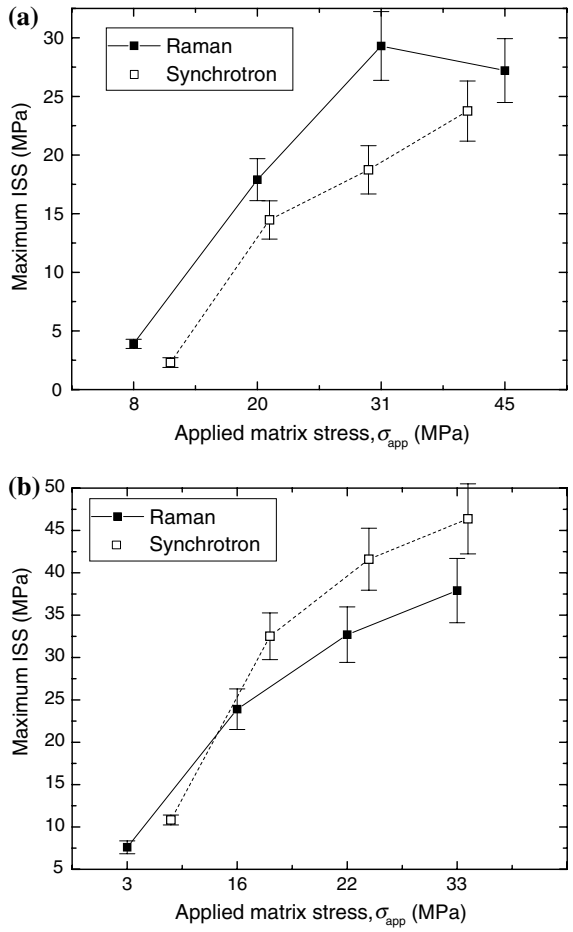

Fig. 13 Comparison of the maximum interfacial shear stress for the Raman and synchrotron methods of determination for (**a**) PPTA and (**b**) PBO fibre-based samples

Distributions of interfacial shear stress derived (and fitted to each data set) using Eq. 4 from the theoretical shear-lag analyses, allowed comparison of the maximum interfacial shear stresses obtained using the synchrotron and Raman techniques. These results, which are summarised graphically for PPTA and PBO specimens in Fig. 13a, b show there is good correlation between the two techniques.

Localised, but significant debonded regions were found in both PPTA and PBO single-fibre embedded model composites whilst conducting the Raman spectroscopy experiments. These are thought to be as a consequence of repeated deformation of the samples to higher stress after the synchrotron analysis.

Finally, it can be concluded that the potential of synchrotron XRD as a tool for monitoring micromechanical behaviour in fibre reinforced composite materials has been successfully demonstrated. This is attributable to the ability to generate high quality diffraction patterns from single high performance rigid-rod polymer fibres, such as PPTA and PBO. Raman spectroscopy has provided the essential confirmation of the validity of the synchrotron radiation approach and vice versa.

Acknowledgements The authors would like to thank Manfred Burghammer at ESRF beamline ID13 for assisting with the experimental set-up. They would also like to thank Teijin and Toyobo for supplying the PPTA and PBO fibre samples, respectively. Our gratitude also extends to Andrew Hammersley for use of the FIT2D software application and colleagues in the Manchester Materials Science Centre who have collaborated with us in this study. This research was supported by the EPSRC (grant code EP/C002164/1).

References

1. Harris B (1999) Engineering composite materials. IOM Communications Ltd
2. Wagner HD, Eitan A (1990) App Phys Lett 56:1965
3. Herrera-Franco PJ, Drzal LT (1992) Composites 23:2
4. Cox HL (1952) Brit J Appl Phys 3:72
5. Young RJ, Eichhorn SJ, Shyng Y-T, Riekel C, Davies RJ (2004) Macromolecules 37:9503
6. Andrews MC, Day RJ, Patrikis AK, Young RJ (1994) Composites 25:745
7. Mccrum NG, Buckley CP, Bucknall CB (1997) In: Principles of polymer engineering. Oxford University Press
8. Kelly A, Tyson WR (1965) J Mech Phys Sol 13:329
9. Piggott MR (1991) Comp Sci Tech 42:57
10. Hammersley AP, Riekel C (1989) Synch Rad News 2:24
11. Davies RJ, Montes-Moràn MA, Riekel C, Young RJ (2001) J Mater Sci 36:3079
12. Young RJ, Lovell PA (1996) In: Introduction to polymers, 2nd edn. Chapman & Hall, London
13. Sakurada I, Nukushina Y, Ito T (1962) J Polymer Sci 57:651
14. So CL, Bennnett JA, Sirichaisit J, Young RJ (2003) Plas Rub Compos 32:199
15. Yeh W-Y, Young RJ (1999) Polymer 40:857
16. Rutledge GC, Suter UW (1991) Polymer 32:2179
17. Montes-Moràn MA, Davies RJ, Riekel C, Young RJ (2002) Polymer 43:5219
18. Andrews MC (1994) In: Stress transfer in aramid/epoxy model composites, PhD Thesis, UMIST, Manchester Materials Science Centre
19. So CL, Young RJ (2001) Composites 32:445